CHAPTER 4 INTERACTION PROCESSES FOR MOLECULES OF INDUSTRIAL RELEVANCE

"This chapter outlines to calculate the electron-induced molecular processes for the compounds furfural, p-benzoquinone, and fluoronitriles that are essential for industry. Fluoronitriles exhibit exceptionally low GWP and have potential uses in plasma reactors and gas discharges. We have computed Q_{inel}, Q_{el} and Q_T through SCOP, from ionization energy (IE) to 5000 eV. Using the CSP-ic method, the continuum and discrete contributions have been computed in terms of ionization (Q_{ion}) and excitation ($\sum Q_{exc}$) cross-sections, respectively. To estimate Q_T, a novel two-parameter semi-empirical method has been proposed and validated. This method is useful for the complex molecular target $55 < Z < 95$. The calculated outcomes are compared with available data. Also, we have calculated the dielectric constant($\mathcal{E}$) using a variety of techniques and correlations with molecular ionization for these applied molecules".

4.1 Introduction

In recent decades, there has been rising global demand in developing novel or enhanced technologies, especially with regard to environmental sustainability and cost-effectiveness, for converting lignocellulosic biomass into various biomaterials [1] including biofuels [2,3]. Radicals and free electrons generated in atmospheric pressure plasmas can promote biomass degradation by inducing excitations, dissociations, and diverse fragmentation processes [4,5]. This conclusion is supported by numerous theoretical and experimental studies that have examined this phenomenon. Thus, we have thoroughly investigated p-benzoquinone ($C_6H_4O_2$) and furfural ($C_5H_4O_2$). Furfural has a wide range of potential uses in the agrochemical, medicinal products, and biofuel sectors, among others. In contrast, p-benzoquinone is a critical compound with widespread applications in cutting-edge technologies, such as energy storage devices, pseudocapacitive systems, artificial photosynthesis, rechargeable battery development, and the design of novel electronic components. Its versatile redox properties make it an indispensable material for advancing sustainable and efficient energy solutions. Moreover, we have studied the effects of electron collisions on Furfural, a byproduct of certain lignocellulosic species that holds potential as a substitute for petroleum-based compounds [6].

The scientific community widely acknowledges and recognizes furfural as a critical chemical compound, as demonstrated by numerous studies [6,7,8]. It plays a key role in advancing the commercialization and operational efficiency of bio-refineries. To achieve significantly higher biofuel yields, it is essential to subject biomass to pre-treatment processes using advanced techniques like electron beam irradiation or atmospheric pressure plasma technologies [3,4]. This insight, along with various modeling applications involving plasma technologies [9], highlights the urgent need for precise and detailed data on electron scattering processes, particularly for the chemical compound furfural [10].

Oxygenic photosynthesis is the primary mechanism driving energy conversion on Earth. This intricate biochemical process involves the transformation of water (H_2O) and carbon dioxide (CO_2) into molecular oxygen (O_2) and carbohydrates, commonly referred to as sugars. Gaining a deeper understanding of the complex pathways within photosynthesis has the potential to accelerate advancements in photocatalysis & photovoltaics, and lead to improvement in hybrid technologies that combine irradiated electro-chemical systems of biological relevance. Among the key components of photosynthesis, quinones are important in cellular respiration and the

electron transport chain due to their exceptional capacity for reversible reduction reactions, which significantly contribute to the efficiency and functionality of the process.

The schematic of the molecules is depicted in figure 4.1.

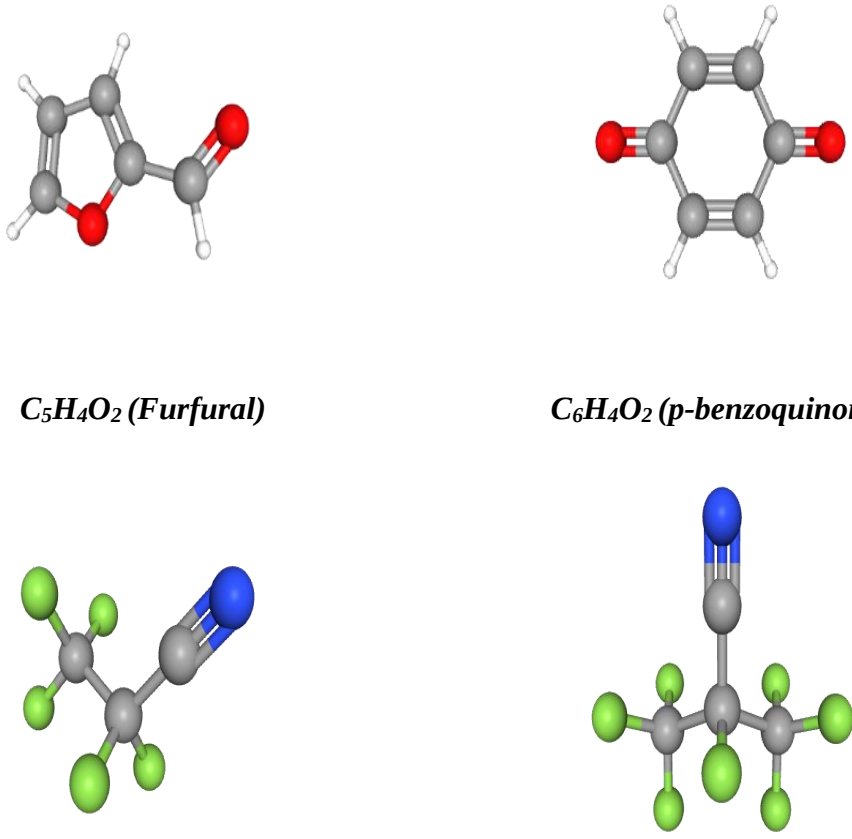

Figure 4.1 Applied molecules (https://pubchem.ncbi.nlm.nih.gov)

4.2 Furfural ($C_5H_4O_2$)

In this section we have focused on Furfural ($C_5H_4O_2$) which have gained recent interest. This section is categorized by three subsections including motivation, previous work along with molecular properties and results of furfural.

4.2.1 Motivation

Furfural ($C_5H_4O_2$) is a crucial part of green chemistry and is also used in plastics, agrochemicals, petroleum, and pharmaceuticals. Consequently, they are emerging as a sustainable and cost-efficient material for long-term use in energy harvesting mechanism, including plasmonic light harvesting, artificial photosynthetic, phototransistors, dye-sensitized solar cells, pseudo capacitors, and batteries [14].

4.2.2 Previous work and molecular properties

The previous studies are shown in the Table 4.1 on furfural.

Table 4.1 Previous work on Furfural

Mol.	Qty.	Method of investigation	E_i (eV)	Ref.
Furfural	Q_{ion}	BEB	1-1000	[10]
	Q_{inel}, Q_{el}, Q_T	IAM-SCAR+I		
	Q_{exc}	Energy loss spectra	20,30,40,50,250	
	Q_{exc}	Discrete inelastic	1-1000	
	Q_T	Electron transmission technique	10-1000	[15]
	Q_T	SEM & IAM-SCAR+I	500 to10000	
	Q_T	Electron Transmission	7, 10, 20	[16]

The molecular properties are show in table 4.2 for furfural.

Table 4.2 Molecular properties

Target	IP (eV)	Polarizability (α)	
		($A^{\circ 3}$)	**($a.u.^3$)**
Furfural ($C_5H_4O_2$)	9.21	10.0	67.55

4.2.3 Results

This section quantifies electron impact cross sections with molecules across an energy ranging from the ionization threshold up to 5000 eV. These cross sections are categorized into two main types: (i) Inelastic CSs (ii) Elastic CSs.

(i) Inelastic CSs

The results of present ionization, inelastic, and excitation CSs for furfural are illustrated in figure 4.2. The upmost curve of Q_{inel} is compared with the only available data of [10]. They have used IAM-SCAR+I [10] for energies from 1 eV to 1000 eV. Throughout the energy range present Q_{inel} shows excellent accord with that of [10] except at the peak region, where present Q_{inel} slightly overestimates the IAM-SCAR+I result. Jones and coworkers [10] have reported the Q_{ion} results using BEB and present data are seen to be in good accord with them within the mentioned 15% uncertainty of BEB [20]. The curve that is positioned at the bottom of the graphical representation distinctly illustrates the calculated $\sum Q_{exc}$. It is compared with both theoretical and experimental excitation cross sections of [10].

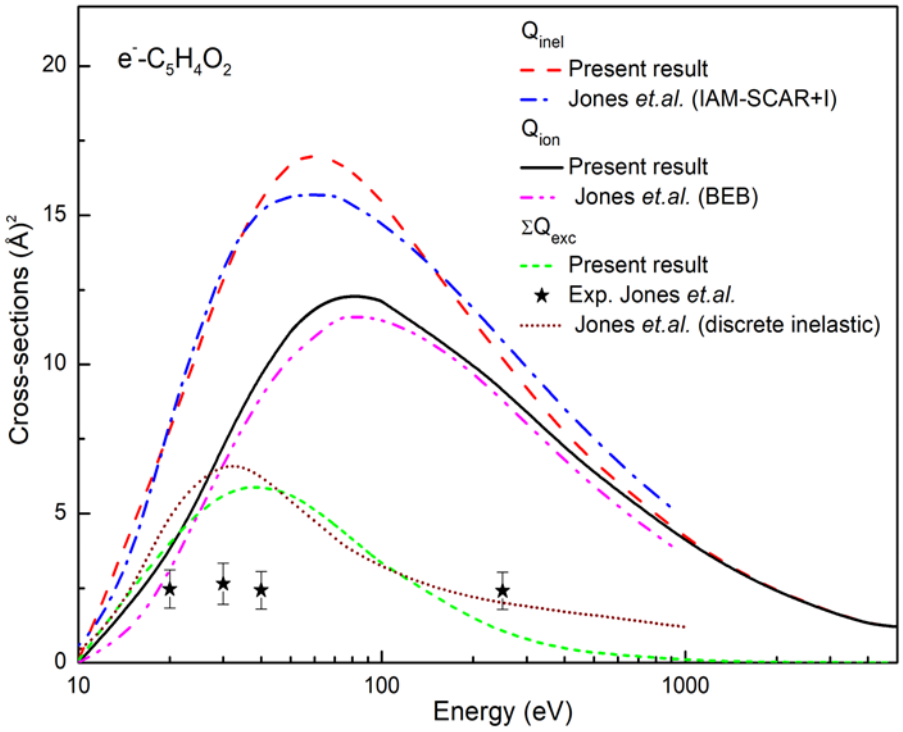

Figure 4.2: Q_{inel}, Q_{ion}, and $\sum Q_{exc}$ for e-$C_5H_4O_2$

Q_{inel}: Dash - Present, Dash dot - [10]**, Q_{ion}: Solid - Present, dash dot dot** - [10]**, Q_{exc}: short dash-Present, filled star**- [10]**, short dot**- [10]

The current $\sum Q_{exc}$ values are consistent with theoretical estimations, but slightly exceed the experimental results reported by [10]. Authors [10], reported electronic excitation CSs for bands I-VI, along with the summed excitation cross section ($\sum Q_{exc}$) spanning 20-250 eV. The reported data had an uncertainty range of 18% to 69%.

(ii) Elastic cross sections

The figure 4.3 presents the computed elastic and total CSs using the present theories. The available Q_{el} data from [10] is compared with the present results. A noticeable deviation at low energies is observed, attributed to the inclusion of inelastic channels in the current Q_{el} calculations, whereas [10] computed pure elastic cross sections. The authors [10], also noted that the inclusion of an interference component in their elastic cross-section calculations introduced an uncertainty of up to 43% at 1 KeV. Additionally, the Q_T computed using the SCOP method in this study is plotted in Figure 4.2 and compared with existing data from [10,15,16].

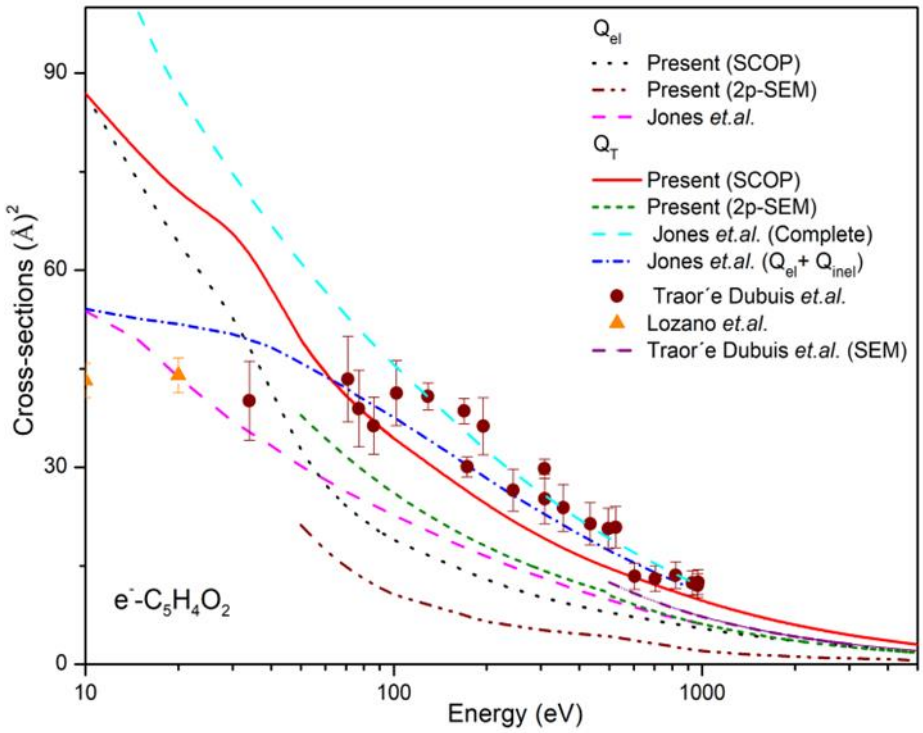

Figure 4.3 Q_{el} and Q_T for e-$C_5H_4O_2$

Q_{el}: Dot -Present (SCOP), Dash dot dot -Present (2p-SEM), Dash -[10], Q_T: Solid - Present (SCOP), Short dash- present (2p-SEM), Dash - [10], Short dash dot- [10], solid circle- [15], Solid triangle- [16], Dash - [15]

The observable discrepancies between the current dataset and all previously available datasets can be clearly identified and analyzed using the graphical representation provided in figure 4.3. Nevertheless, it is noteworthy that the results obtained from the current analysis of Q_T demonstrate a consistent trend that aligns closely with the findings reported in [10]. Although the calculations performed in the present study do not take into account the effects associated

with non-spherical effect, it is important to highlight that Jones and coworkers [10] have incorporated the consideration of excitation through molecular rotational excitations into their analysis of Q_T. This consideration of rotational dynamics may provide a plausible explanation for the observed discrepancies between the current results and those reported in reference [10]. The experimental Q_T data from [15], with an uncertainty range of 4% to 22% above 50 eV, shows reasonable agreement with the current results. Additionally, for energies above 500 eV, QT values proposed by [21] for molecules with up to 22 electrons have also been determined by Traoré Dubuis and colleagues [15]. The authors pointed out that the SEM model has not been verified for the molecules that have a cyclic structure, with higher atomic numbers. Although the SEM results are underestimated at lower energies, they exhibit a trend consistent with the Q_{el} and Q_T estimates obtained in this study using the 2p-SEM method.

Table 4.33 Total cross section data (Å^2) for Furfural

E_i (eV)	**Q_{ion}**	**Q_{el}**	**Q_T**
10	0.01	86.84	86.92
20	3.40	63.38	70.95
30	7.32	53.77	66.88
40	9.73	41.66	57.34
50	11.10	32.70	49.42
60	11.84	27.51	44.49
70	12.18	24.12	40.93
80	12.28	21.95	38.37
90	12.24	20.20	36.15
100	12.12	18.95	34.40
200	10.05	12.66	24.11

300	8.40	10.19	19.35
400	7.23	8.82	16.53
500	6.37	7.85	14.55
1000	4.06	5.40	9.55
1500	3.02	4.26	7.31
2000	2.40	3.56	5.98
2500	2.01	3.09	5.11
3000	1.72	2.75	4.48
3500	1.49	2.49	3.99
4000	1.33	2.28	3.61
4500	1.25	2.12	3.29
5000	1.20	1.98	3.01

4.3 p-Benzoquinone ($C_6H_4O_2$)

In this section we have focused on p-Benzoquinone (pBQ) which have gained recent interest. This section is categorized by three subsections including motivation, prior studies along with molecular properties and results of p-benzoquinone.

4.3.1 Motivation

The enhancement of bio-inspired devices that are specifically designed for the conversion and harvesting of energy can be significantly improved and accelerated through a comprehensive knolowedge associated with “Quinone and its various derivatives”, as highlighted in the previous research [14]. In this particular view, pBQ, which is recognized as the most fundamental and simplest form of quinone, has effectively functioned as a prototype in a wide

array of scientific research endeavors that aim to elucidate the intricate electro-chemical behaviors exhibited by quinones, as documented in the literature [14].

4.3.2 Previous work and molecular properties

The previous studies on p-benzoquinone are shown in the Table 4.4.

Table 4.4 Previous work on p-benzoquinone

Mol.	Qty.	Method of investigation	E_i (eV)	Ref.
pBQ	Q_{el}	SMCPP	1-50	[17]
	Q_{inel}, Q_{ion}, Q_{el}, Q_T, Q_{exc}	IAM-SCAR+I	1-200	
	Q_T	Transmission beam attenuation measurements		
	Q_{exc}	Energy loss spectra	20,30,40	[18]
	Q_{inel}, Q_{el}, Q_T, Q_{exc}	IAM-SCAR+I	10-1000	
	Q_{ion}	BEB	10-1000	
	Q_{inel}, Q_{el}, Q_T, Q_{ex}	SMCPP	16-50	

The molecular properties are show in table 4.5 for parabenzoquinone ($C_6H_4O_2$).

Table 4.5 Molecular properties

Target	IP (eV)	Polarizability (α)	
		($A^{\circ 3}$)	($a.u.^3$)
Parabenzoquinone ($C_6H_4O_2$)	10.01 [19]	10.8	72.95

4.3.3 Results

The present section covers the elastic and inelastic effects of $C_6H_4O_2$ from the IP energy range to 5keV. Compare with the available comparisons as well. And the cross sections data are displayed in the Table 4.6.

Table 4.64 Total cross section data ($Å^2$) for pBQ

E_i (eV)	Q_{ion}	Q_{el}	Q_T
11	0.02	75.38	75.57
20	3.94	53.92	62.79
30	9.08	37.48	53.66
40	12.16	26.91	46.42
50	13.82	21.12	41.90
60	14.66	17.65	38.68
70	15.03	15.28	36.06
80	15.13	13.64	33.95
90	15.07	12.20	31.92
100	14.91	11.21	30.32
200	12.07	6.92	20.75
300	9.92	5.40	16.26
400	8.43	4.53	13.55
500	7.36	3.91	11.66
1000	4.55	2.49	7.15
1500	3.32	1.88	5.24
2000	2.62	1.55	4.19
2500	2.17	1.32	3.51
3000	1.85	1.16	3.02

3500	1.60	1.04	2.65
4000	1.41	0.96	2.37
4500	1.27	0.89	2.16
5000	1.14	0.84	1.98

(i) Inelastic cross sections

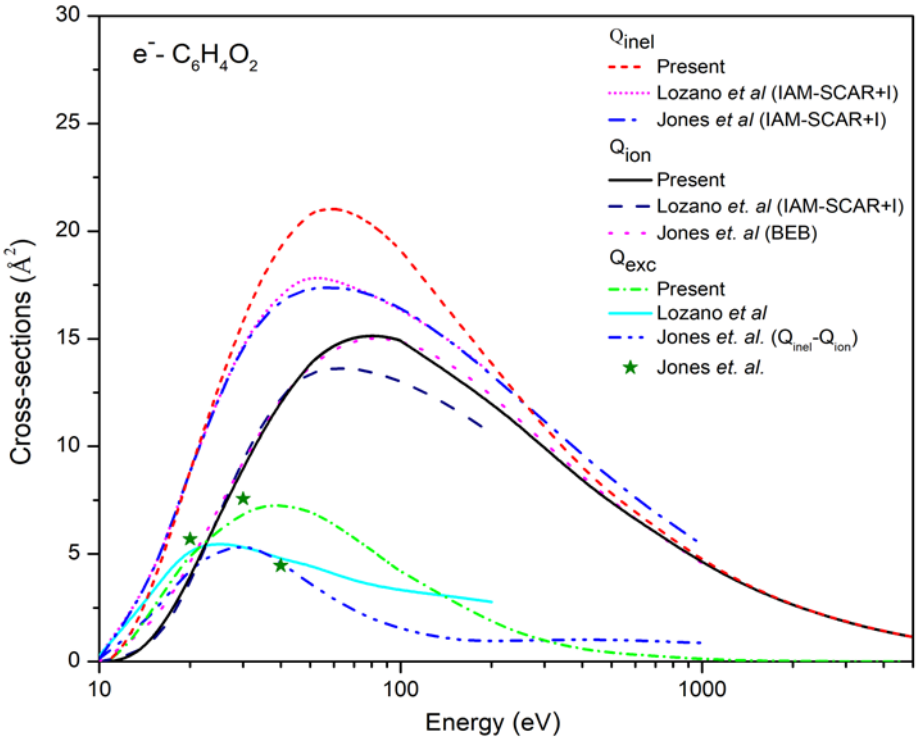

Figure 4.4 : Q_{inel}, Q_{ion}, and $\sum Q_{exc}$ for e-$C_6H_4O_2$

Q_{inel}: short dash -Present, short dot - Lozano *et al* [17], dash dot- [18] (IAM-SCAR+I), Q_{ion}; solid -Present, dash -Lozano *et al* [17], dot - Jones *et at* [18] (BEB), Q_{exc}; short dash dot -present, dash dot dot -Jones *et al* [18], solid star- Jones *et al* [18] (Discrete inelastic)]

The top curve in figure 4.4 shows the inelastic scattering CSs (Q_{inel}) for e-$C_6H_4O_2$ collisions, compared with data from [17,18]. These authors are employed the "IAM-SCAR+I" method for the computations. Our results show good agreement with the existing data, except in the peak region. The present ionization cross sections are also compared with theoretical data from the [17,18], as shown in figure 4.4. Our data of Q_{ion} shows excellent agreement with the results of Jones *et al* [18]. However, the data from [17] underestimates both the present results and those of Jones *et al* [18], especially for energies up to 200 eV. In Figure 4.4, the summation of $\sum Q_{exc}$, calculated using the present methodology is presented alongside comparative data for validation. The excitation cross sections computed theoretically using the "IAM-SCAR+I"approach [17,18] agree well with the current results at energies lower than 25 eV but are smaller than the present $\sum Q_{exc}$ at higher energy levels. Furthermore, Jones *et al* [18] conducted measurements of the electronic excitation CSs for individual bands 0 through V over the energy range of 20 to 40 eV, providing detailed insights into the excitation behavior within this interval. The summation values for these bands are compared to the present $\sum Q_{exc}$ and show reasonable agreement at 20 eV and 30 eV.

(ii) Elastic cross sections

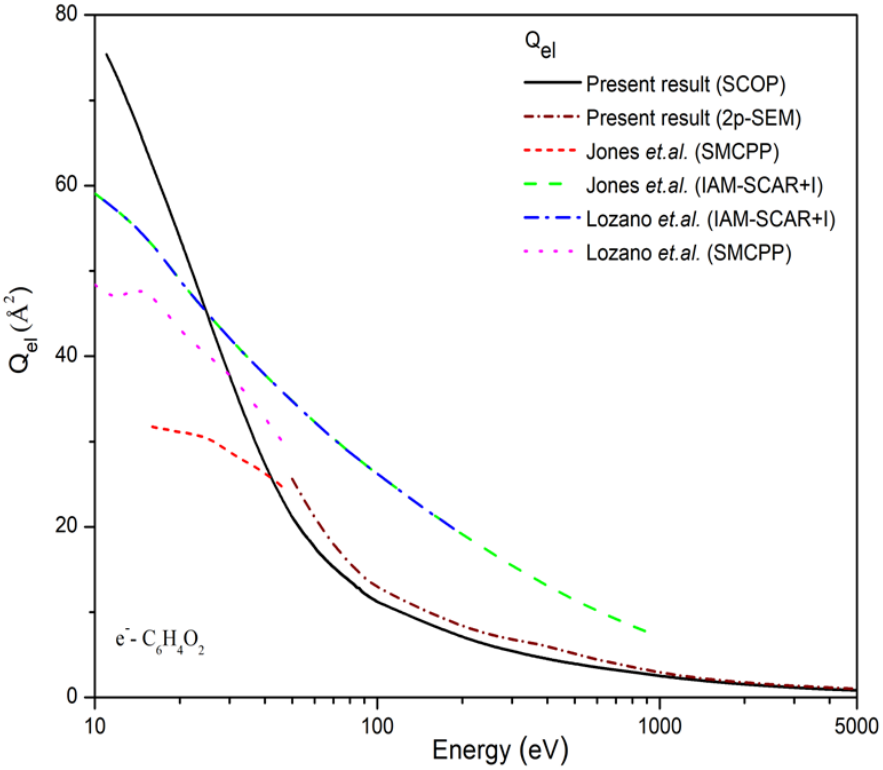

Figure 4.5 Q_{el} for e-$C_6H_4O_2$

Q_{el}: Solid - Present (SCOP), short dash- Present (2p-SEM), Dot- Lozano *et al* [17] (SMCPP), dash dot -Lozano *et al* [17] (IAM-SCAR+I), dash- Jones *et at* [18] (IAM-SCAR+I), short dash- Jones *et at* [18] (SMCPP)

The Figure 4.5 displays the present Q_{el} for e-$C_6H_4O_2$ alongside available elastic results obtain through the SMCPP [17,18] and IAM-SCAR+I [17,18] methods. The present data slightly overestimates the theoretical results up to 30 eV. On the other hand, the reported results tend to overestimate the present data up to 30 eV. For energies above 30 eV, the present CSs align closely with the data from Lozano and coworkers [17] and Jones coworkers [18], which were obtained using the SMCPP method, while underestimating the data from [17]. The 2p-SEM formalism results show excellent agreement with the SCOP data.

(iii) Total cross sections

The comprehensive total cross-sections, calculated as part of this study, are presented in figure 4.6. These results are compared alongside the corresponding data available from previously published studies and experimental measurements.

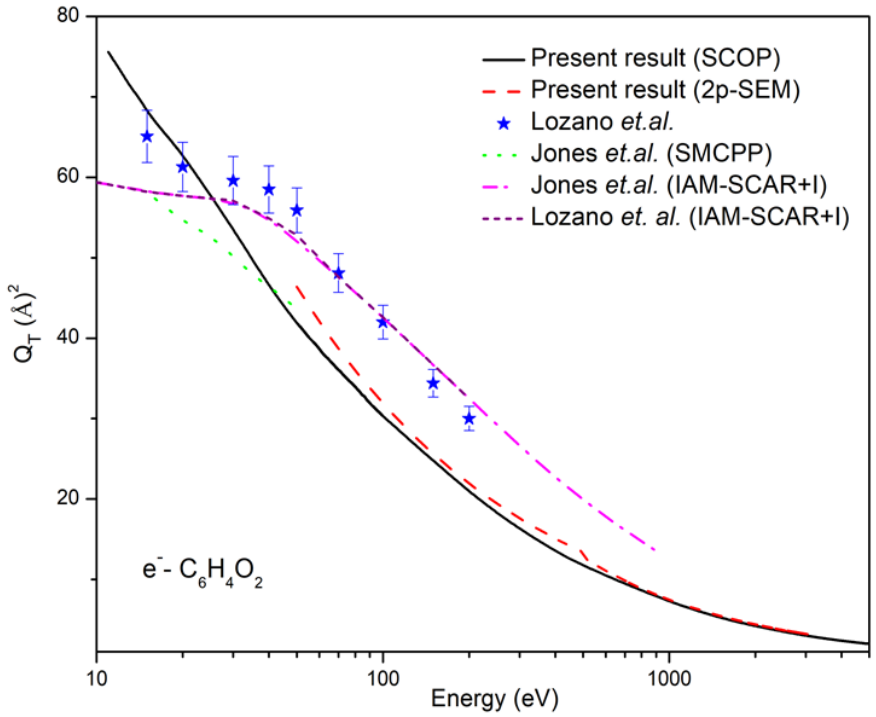

Figure 4.6 Q_T for e-$C_6H_4O_2$

Q_T: solid- Present, dash- Present (2p-SEM), solid star- Lozano *et al* [17] (Exp.), dot - Jones *et al* [18] (SMCPP), dash dot - Jones *et al* [18] (IAM-SCAR+I), short dash - Lozano *et al* [17] (IAM-SCAR+I)

From the IP to 30 eV, present data show excellent matching with experimental results [17] within the uncertainty limit of ±5%, but they understate theoretical results calculated through [17]. The results obtained using the 2p-SEM method exhibit remarkable agreement with the SCOP data, demonstrating a high level of consistency between the two approaches. Furthermore, the present findings from both SCOP & 2p-SEM reveal with a similar overall pattern with previous datasets. This alignment underscores the reliability of the current methodologies and their congruence with previously reported results in the literature.

4.4 Fluoronitrile molecules

This study provides an in-depth analysis of Fluoronitrile molecules, investigating their properties from ionization potential to 5000 eV. It reports the probabilities of various processes triggered by electron incidents [29,30], emphasizing their environmental importance and relevance to plasma.

4.4.1 Motivation

Sulfur hexafluoride (SF_6) is commonly used as an insulating agent in high-voltage systems [22]. Several more physico-chemical properties include low boiling point, good insulating agent and non-toxicity. However, sulfur hexafluoride (SF_6) possesses a significantly higher "Global warming potential (GWP)" compared to carbon dioxide (CO_2), making it a much more potent greenhouse gas. Additionally, (SF_6) is remarkably stable and degrades at an exceedingly slow rate in the environment, contributing to its long atmospheric lifetime and amplifying its environmental impact over time.

As a result, finding a substitute gas for SF_6 is the most pressing problems in the field of mechatronics study.

Equipment insulation utilizing SF_6 is commonly employed in ultra-high-voltage electrical systems due to its exceptional insulating and arc-quenching characteristics. However, the failure of this insulation system could result in substantial financial losses, including the costs associated with equipment damage, system downtime, and potential safety hazards. Such risks underscore the critical importance of ensuring the reliability and integrity of SF_6-insulated devices in these high-stakes applications.

Potential SF_6 replacements, such as fluoronitrile (C_4F_7N, C_3F_5N) compounds, have been carried out an enormously [23–25] in recent years.

Table 4.7 Dielectric strength and GWP

Molecule	GWP	ε_r (rel. SF_6)
SF_6	23900 [28]	1
C_3F_5N	-	2 [26]
C_4F_7N	2100 [27]	2.74 [27]

The dielectric strength and GWP of all of these three molecules have been compared and listed in Table 4.7. Both fluoronitrile gases possess lower GWP [55] and high dielectric strength [56] as compared to the famous SF_6.

A comprehensive dataset of electron-induced collisional CSs are essential for accurately modeling of fluoronitrile behavior in diverse plasma environments, including plasma reactors, gas discharges, and high-voltage insulation systems.

However, very few studies have explored electron interactions with Fluoronitriles, and a literature review indicates a lack of data on elastic CSs (Q_{el}) and total CSs (Q_T), as highlighted in Table 4.5.

4.4.2 Literature survey

The previous studies of electron interaction with Fluoronitriles (C_3F_5N and C_4F_7N) are shown in the Table 4.8.

Table 4.8 Prior investigations into the scattering of electrons by fluoronitrile

Molecules	**Qty.**	**E_i**	**Ref.**
C_3F_5N	Q_{ion}	IE-1000 eV	Wang and coworkers [26]
C_4F_7N	Q_{ion}	IE-1000 eV	Wang and coworkers [26]
	Q_{ion}	IE-2000 eV	Xiong and coworkers [31]
	Q_{ion}	IE-100 eV	Rankovic and coworkers [32]
	Q_{inel}, Q_{ion}, ΣQ_{exc}	IE-5000 eV	Sinha and coworkers [33]

4.4.3 Results for Pentafluoropropionitrile (C_3F_5N)

The complete set of inelastic and elastic CSs for e- C_3F_5N have been reported here.

(i) Inelastic CSs

In figure 4.7 shows present Q_{inel}, Q_{ion} and $\sum Q_{exc}$ for e-C_3F_5N along with earlier research.

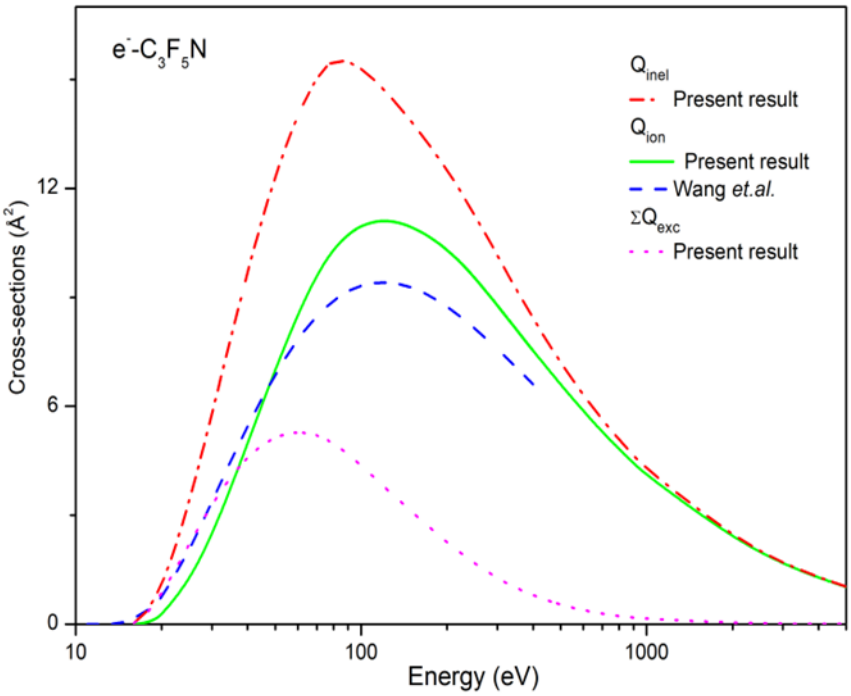

***Figure 4.7* Q_{inel}, Q_{ion}, and $\sum Q_{exc}$ *for* C_3F_5N**

Dash dot: Present Q_{inel}; Solid: Present Q_{ion}; Dash: Q_{ion} [34]; Dot: Present $\sum$Qexc

As shown in figure 4.7, the our ionization CSs Q_{ion} for C_3F_5N coincides very well with the data of [34] throughout the wide energy range. Quite apart from the reported error of 10% in the BEB results [35,36], we find that our Q_{ion} values climb more gradually and are greater overall than the BEB data from the threshold on up. The bottom curve is ΣQ_{exc}, for which there is no literature comparison, while the top Q_{inel} curve includes electronic excitations and ionization.

(ii) Total and elastic CSs

In figure 4.8, the present elastic Q_{el} & total Q_T CSs for the molecule C_3F_5N are depicted. The results demonstrate that the two theoretical approaches utilized to compute the cross-sections exhibit excellent agreement over the entire investigated energy range. This consistency highlights the robustness of the applied methodologies in accurately modeling the scattering behavior of C_3F_5N. Both sets of results are calculated using two methods: the SCOP approach and the 2p-SEM formalism. Throughout the entire energy range of 2p-SEM (50-10,000 eV), the results from both methods are observed to overlap. However, there are no previously reported data for Q_{el} and Q_T available for comparison.

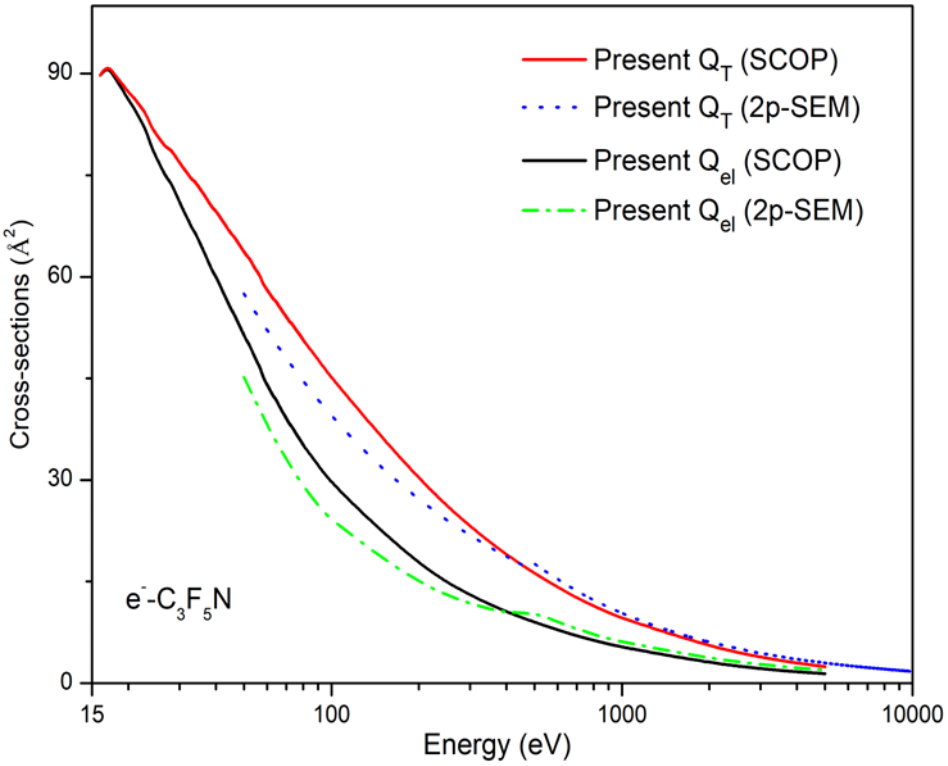

Figure 4.8 Q_{el} for e-C_3F_5N

Solid: Present Q_T (SCOP); Dotted: Q_T Present(2p-SEM); dash: Q_{el} Present(SCOP); dash dot: Q_{el}- Present(2p-SEM)

The cross sections data are tabulated for e-C_3F_5N in Table 4.9.

Table 4.9 Total CSs ($Å^2$) for C_3F_5N

E_i (eV)	Q_{ion}	Q_{el}	Q_T
16	0.00	89.72	89.74
20	0.25	86.14	87.25
30	2.46	71.10	76.89
40	4.98	60.05	69.73
50	7.00	51.41	63.72
60	8.51	44.08	58.07
70	9.60	39.05	54.07
80	10.30	35.11	50.63
90	10.72	32.24	47.88
100	10.96	29.41	44.99
200	10.30	17.24	29.91
300	8.78	12.96	23.10
400	7.54	10.54	18.94
500	6.60	9.02	16.22
600	5.87	7.90	14.21
700	5.29	6.99	12.62
800	4.83	6.34	11.43
900	4.44	5.79	10.44

1000	4.10	5.32	9.59
2000	2.37	2.99	5.40
3000	1.66	2.14	3.82
4000	1.28	1.69	2.98
5000	1.03	1.42	2.45

4.4.4 Results for Heptafluorobutyronitrile (C_4F_7N)

In this section, the electron impact various interaction processes are shown discussed. In figure 4.9 shows inelastic effect and figure 4.10 shows elastic effect along with the available comparison.

(i) Inelastic Processes

In figure 4.9, the inelastic scattering effects for the molecule C_4F_7N are illustrated. The figure includes the inelastic CSs (Q_{inel}), the ionization CSs (Q_{ion}), and the summed excitation CSs (ΣQ_{exc}).

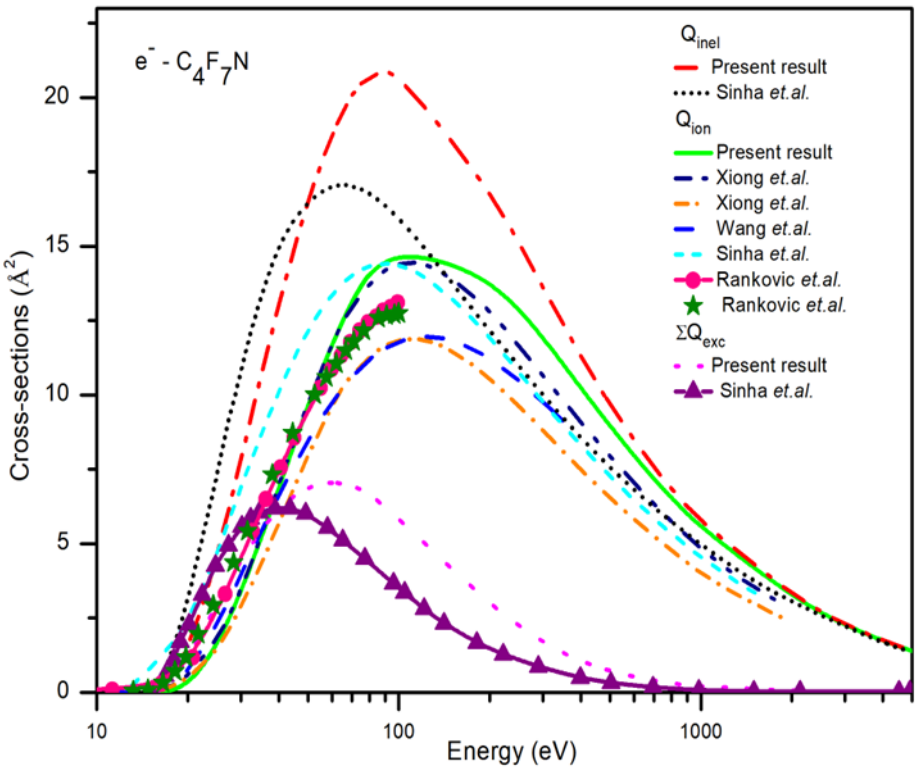

Figure 4.9 Inelastic processes for e-C_4F_7N

Solid: Q_{ion}(Present); Dashed: Wang and coworkers[26]; Dash Dot Dotted: Xiong and coworkers [31]**; Short Dashed Dot: Xiong and coworkers** [31]**; Short Dashed: Sinha and coworkers** [33] **Q_{ion}; -●- Rankovic and coworkers** [32] **Q_{ion}; Star- Rankovic and coworkers** [32] **Q_{ion}; Dash Dotted: Present Q_{inel}; Short Dotted : Sinha and coworkers** [33] **Q_{inel}; Dotted:Present ΣQ_{exc}; -◄- line: Sinha and coworkers** [33] **ΣQ_{exc}**

The present inelastic, ionization, and excitation CSs for C_4F_7N are shown in figure 4.9. The uppermost curve is represented present Q_{inel} , which have larger magnitude than the data given by Sinha et al. [33]. The present Q_{ion} data aligns well with existing data [31] from the ionization threshold up to 40 eV, with the exception of the results from Sinha et al. [33]. The discrepancy observed between the Q_{ion} values from Sinha et al. and other studies may be attributed to their inclusion of nuclear charge effects in the molecule. In the peak region of Q_{ion}, the current results closely match the Q_{ion} data obtained using the modified DM formalism [31]. Beyond the peak, the ionization cross-section Q_{ion} values obtained from the Binary-Encounter-Bethe (BEB) and Deutsch-Märk (DM) calculations are slightly lower than those reported in existing datasets. However, both theoretical approaches exhibit a reasonable level of agreement with the available data up to the Q_{ion} maximum, indicating their reliability in capturing the ionization

behavior within this energy range. Additionally, at low energies, the current Q_{ion} results exhibit excellent agreement with the experimental Q_{ion} data reported by Ranković et al. [32].

(ii) Elastic processes

Present Q_{el} and Q_T CSs data for the C_4F_7N compound are illustrated in figure 4.10. The results were obtained through the SCOP approach and the 2p-SEM formalism. For this molecule, the data from both methodologies gives excellent agreement. However, there are no available previously reported Q_{el} and Q_T data for comparison. The CSs data are displayed for C_4F_7N in table 4.10.

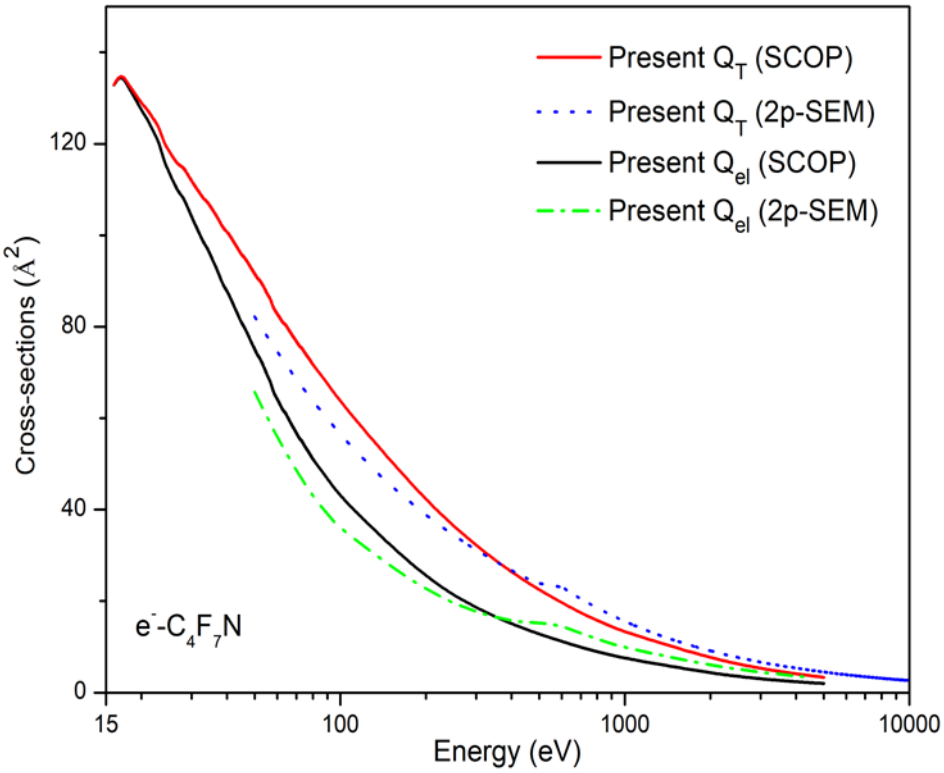

Figure 4.10 Elastic processes for e-C_4F_7N

Q_T- Red solid: Present SCOP; Blue dotted: Present 2p-SEM; Q_{el}- Black solid: Present SCOP; Dash Dotted: Present 2p-SEM

Table 4.10 CSs (Å^2) data for Heptafluorobutyronitrile

E_i (eV)	Q_{ion}	Q_{el}	Q_T
16	0.00	132.88	132.93
20	0.36	127.32	128.86
30	3.41	104.13	111.96
40	6.86	87.86	100.85
50	9.62	75.10	91.57
60	11.66	64.10	82.81
70	13.13	56.78	76.85
80	14.00	51.04	71.75
90	14.49	46.89	67.77
100	14.95	42.58	63.36
200	14.05	24.69	41.66
300	11.95	18.52	32.13
400	10.24	15.00	26.29
500	8.96	12.82	22.49
600	7.97	11.22	19.71
700	7.17	9.90	17.46
800	6.55	8.98	15.82
900	6.01	8.19	14.45
1000	5.56	7.52	13.27

2000	3.20	4.22	7.46
3000	2.25	3.00	5.27
4000	1.74	2.37	4.11
5000	1.39	1.98	3.37

4.5 Correlation study: prediction of polarizability & dielectric constant and validation of novel 2p-SEM

Numerous researchers are working on theoretical advancements to counterbalance the lack of experimental results and the improved circumstances, but many complex targets still present difficulties. Recent theoretical advancements have resulted to innovative sophisticated methods, including the BEB[20], IAM-SCAR+I [37], SCOP[23,41] , ab-initio R-matrix method [40], and complex Kohn & Schwinger multichannel[41,42] methods, to accurately describe interaction electron with molecule.

The aforementioned models are utilized to predict total cross-sections (CSs) resulting from electron impact, while maintaining a balance between accuracy and computational efficiency. These models employ theoretical frameworks that simplify the underlying physical processes without compromising the reliability of the predictions, making them well-suited for extensive cross-section calculations within feasible computational limits.

4.5.1 Prediction of polarizability

In figures 4.11 to 4.15, we have analyzed the present results on total cross-section data obtained using 2p-SEM by plotting correlation graphs for various molecules, including DNA/RNA bases, Furfural, and pBQ with atomic numbers (Z) ranging from 55 to 95.

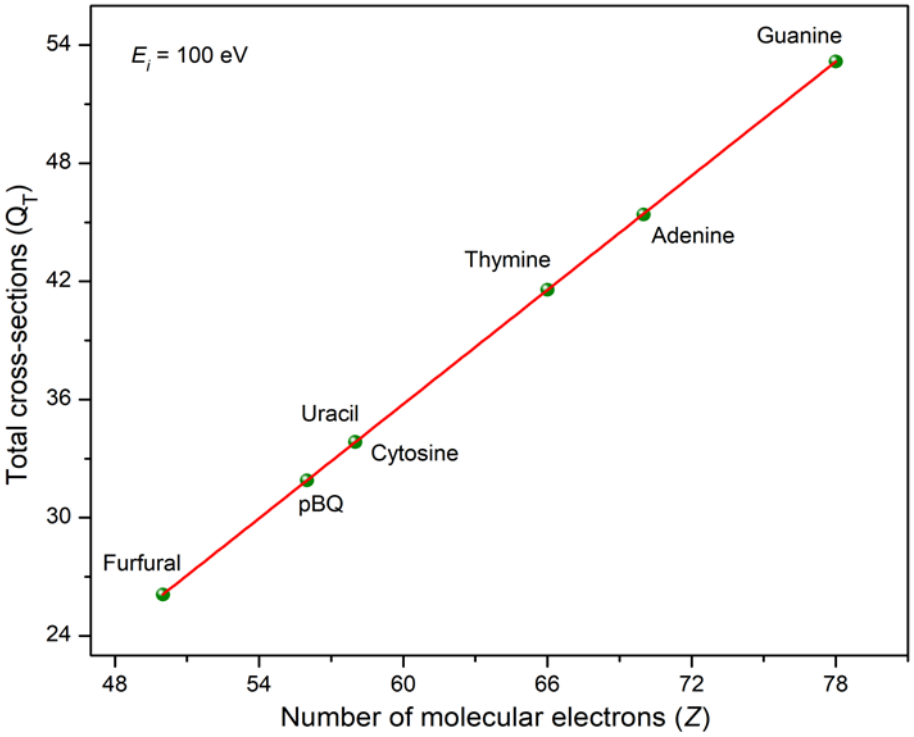

Figure 4.11 Correlation with present Q_T through 2p-SEM and Z

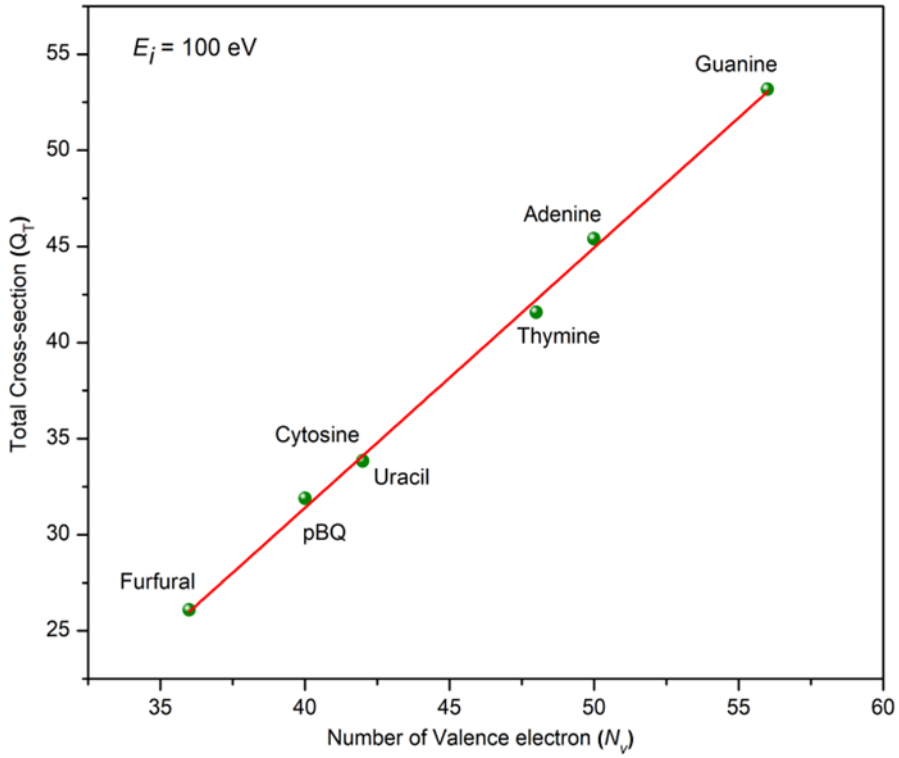

Figure 4.12 Correlation with Q_T through 2p-SEM and N_v

Correlation analysis serves as a crucial tool for evaluating the consistency and reliability of cross-sectional data, particularly in cases where no comparative datasets are available from other research groups. By employing the 2p-SEM method, it is possible to achieve accurate calculations of total CSs (Q_T) and elastic CSs (Q_{el}) for large and complex molecular targets with atomic numbers in the range $55 < Z < 95$. This method is highly effective across a broad energy range, making it a robust approach for studying intricate systems.

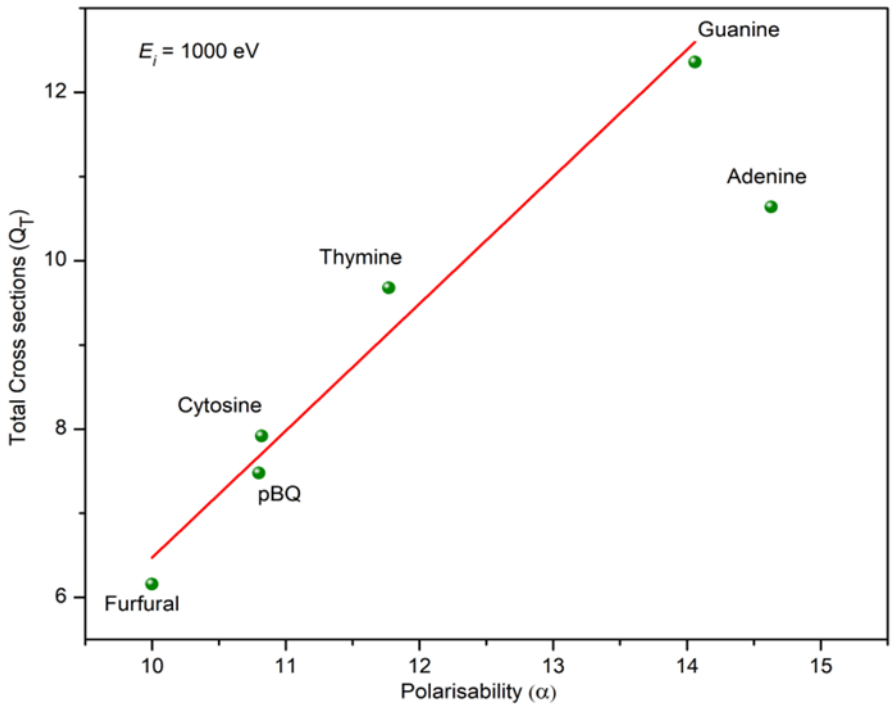

Figure 4.13 Correlation between Q_T and α

To assess the consistency of our 2p-SEM data, we plotted the total scattering cross-section (Q_T) against the target atomic number (Z) and the number of valence electrons (n_v) at an incident electron energy of 100 eV (Figures 4.11 and 4.12).

We observed a strong correlation between the total scattering CSs and the target's charge cloud size, indicating a clear size dependency. And also, we have plotted graph of Q_T vs polarizability (α) in figure 4.13 at 1000 eV. Further, in figure 4.14, we have shown exact correlation with Q_{ion}^{Peak} and target polarizability.

To validate the self-consistency of the current data, we have plotted several graphs. In figures 4.11 and 4.12, the total cross-sections (Q_T) obtained using the 2p-SEM method are plotted as functions of the number of target electrons (Z) and the number of valence electrons (n_v), respectively, at 100 eV. These plots demonstrate a precise correlation, highlighting the size

dependency of the target's charge cloud. Additionally, in figure 4.13, a graph of Q_T versus polarizability (α) is presented at 1000 eV, further emphasizing the relationship between cross-sections and molecular polarizability. Finally, figure 4.14 illustrates a linear correlation between the ionization peak cross-section Q_{ion}^{Peak} and the target polarizability, reinforcing the dependence of ionization behavior on polarizability.

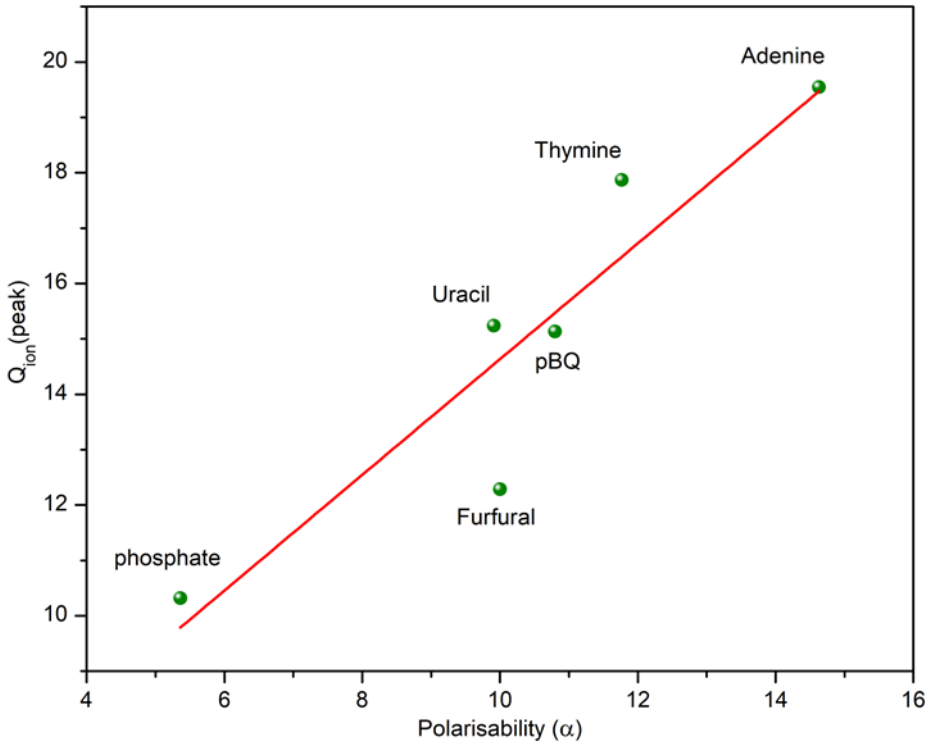

Figure 4.14 Correlation with Q_{ion}^{Peak} and α

We have analyzed the polarizability and other properties of C_3F_5N, C_4F_7N and PFK [44] molecules, which are reported in the literature and investigated in this study. By examining the correlations between these properties and the total "number of electrons" (Z), we can estimate the polarizability of fluoroketone and fluoronitrile molecules. The total "number of electrons" (Z) directly relates to the size of the molecular charge cloud.

Table 4.11 Target properties and estimated **polarizability (*α*)**

Target	IE (eV)	Z	α (10^{-24}cm^{-3})		
			Presented	Estimated	Ref. [a]
C_3F_5N	15.21 [34]	70	5.71 [45]	5.97	6.6
C_4F_7N	15.10[12]	94	6.82 [45]	7.60	8.5
$C_5F_{10}O$	12.02 [46]	128	8.83 [47]	9.84	10.6
$C_6F_{12}O$	11.41 [48]	152	11.44 [49]	12.54	12.6

[a] www.chemspider.com

Figure 4.15 illustrates the relationship between the peak ionization CSs (Q_{ion}^{peak}) and the "number of electrons(Z)" in the target molecule.

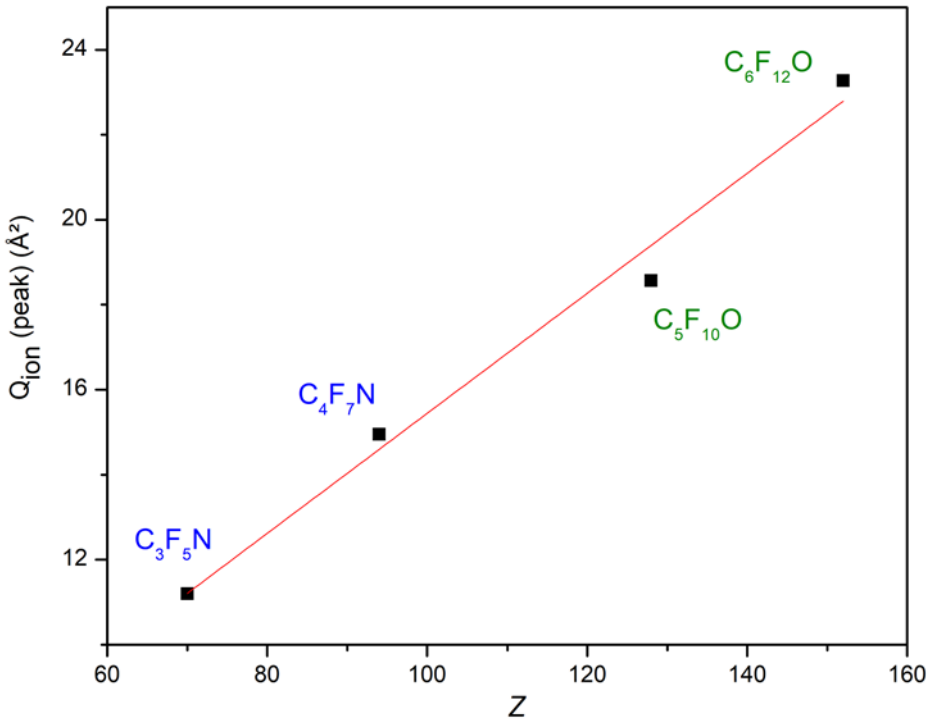

Figure 4.15 Correlation of Q_{ion}^{peak} with Z

The Q_{ion}^{peak} of the target molecule is significantly impacted by the size dependency determined by the number of electrons (Z). As the molecular charge cloud expands, the energy-specific CSs for impact processes increase dramatically. While the initial ionization potential, which remains relatively constant for large molecules (Table 4.8), also influences the ionization cross-section (Q_{ion}). Consequently, figure 4.15 shows a linear relationship between Q_{ion}^{peak} and Z.

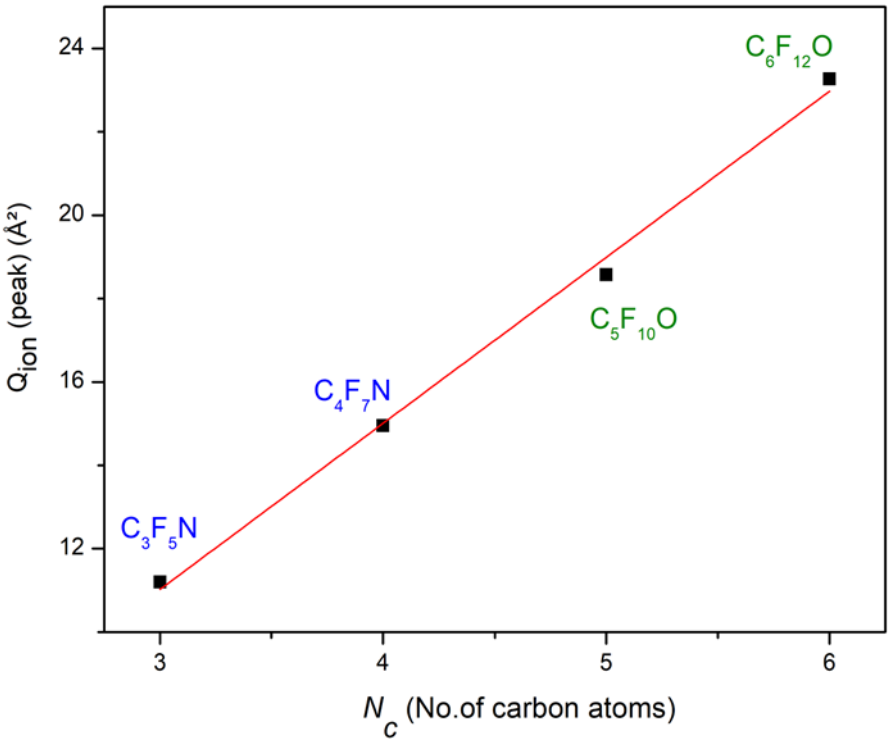

Figure 4.16 Variation of Q_{ion}(peak) with N_c

In Figure 4.16, a similar trend is observed between Q_{ion} (peak) with the N_c (no. of carbon atoms) in the target for fluoronitriles and fluoroketones. By using the study of these dependence and using extrapolation, we can estimate the peak ionization Q_{ion} (peak) CSs for large and complex targets. The Q_{ion} (peak) of such big molecules can be predicted using these relationships and a little extrapolation.

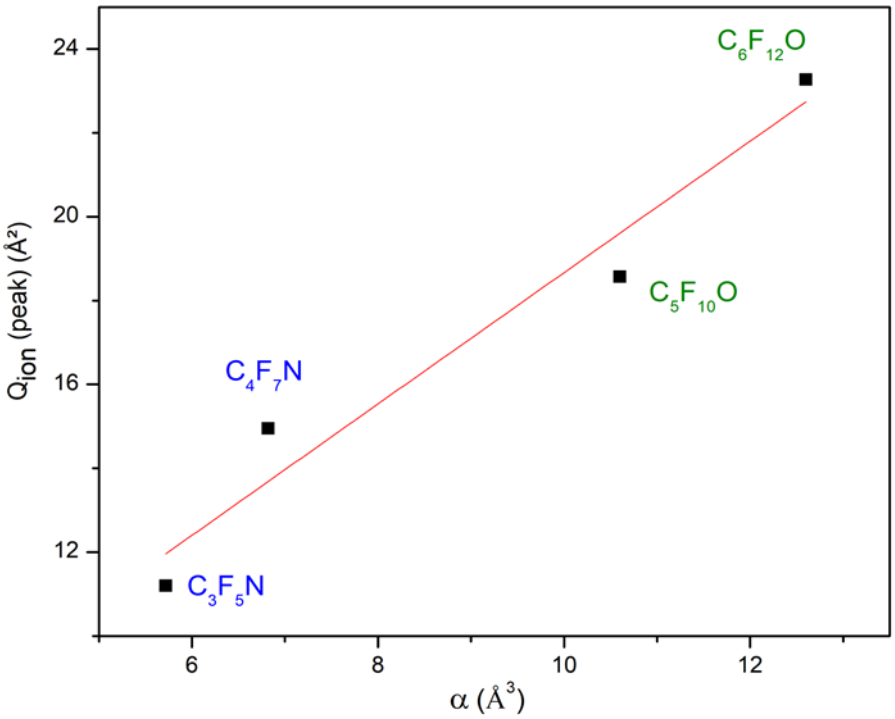

Figure 4.17 Variation of Q_{ion}(peak) with α

We identified a clear linear relationship between the Q_{ion}(peak) and α in figure 4.17. This correlation provides a reliable method for predicting one parameter when the other is known, which is particularly useful for materials where direct measurements are challenging. In Table 4.8, we compare the predicted polarizability values, derived using this relationship, with previously established data. The results show an excellent match between the predicted and existing polarizability.

4.5.2 Computation of dielectric constant, ε

Owing to numerous prospective applications, the investigation of dielectric properties is highly beneficial for p-benzoquinone and furfural, encompassing energy storage systems, pseudocapacitors, phototransistors, solar cells sensitized through dye, artificial photo-synthesis, reuseable batteries, and the advancement of novel electrical and electronic instruments.

The Clausius-Mossotti [51] yields,

$$\frac{\varepsilon-1}{\varepsilon+2} = \frac{4\pi}{3} * N * \alpha \qquad (4.1)$$

Where, N is the no. density of molecule, and α is the dipole polarizability.

The number density is obtained through the following [52],

$$N = \frac{N_A * \rho}{M} \quad (4.2)$$

In the above equation 4.2, N = Number density of target, N_A = Avogadro number, ρ = Density of the substance, M =molar mass.

The mathematical representation of the Onsager [53] gives,

$$\frac{\varepsilon-1}{\varepsilon+2} = \frac{4\pi}{3}\alpha N + \frac{(\varepsilon-\varepsilon_\infty)(2\varepsilon+\varepsilon_\infty)}{\varepsilon(\varepsilon_\infty+2)^2} \quad (4.3)$$

Where, ε_∞ is the high frequency dielectric constant.

Relation between $Q_{ion^{Max}}$ and dielectric constant (ε)

The high frequency dielectric constant denotes as, ε_∞ .

- **Correlation with $Q_{ion^{Max}}$ with dielectric constant (ε)**

As per the Harland's [54] suggestion the Q_{ion}^{Max} with its polarizability (α) is calculated using the equation 4.4,

$$Q_{ion^{Max}} = 11.92(\alpha) = 11.92\left(\frac{3*\left(\frac{\varepsilon-1}{\varepsilon+2}\right)}{4\pi N*IE}\right)^{0.5} \quad (4.4)$$

Table 4.12 Various properties

Mol.	α (10^{-24} cm^3)	$Q_{ion^{Max}}$ (Å^2)	ρ g/cm^3	M g/mol	N cm^{-3}	ε		
						Using eq. 4.1	Using eq. 4.3	Using eq. 4.4
$C_6H_4O_2$	10.8	15.13	1.32	108.1	$7.35x10^{21}$	2.49	1	1
$C_5H_4O_2$	10	12.28	1.16	96.1	$7.27x10^{21}$	2.31	0.99	1

We have employed three well established methodologies (i) Clausius-Mossotti [51] (ii) Onsager [53] and (iii) Harland and Vallance [54] (through eq. 4.1, 4.3, 4.4 respectively), to compute the dielectric constant for the investigated targets. The calculated dielectric constant are presented in table 4.12.

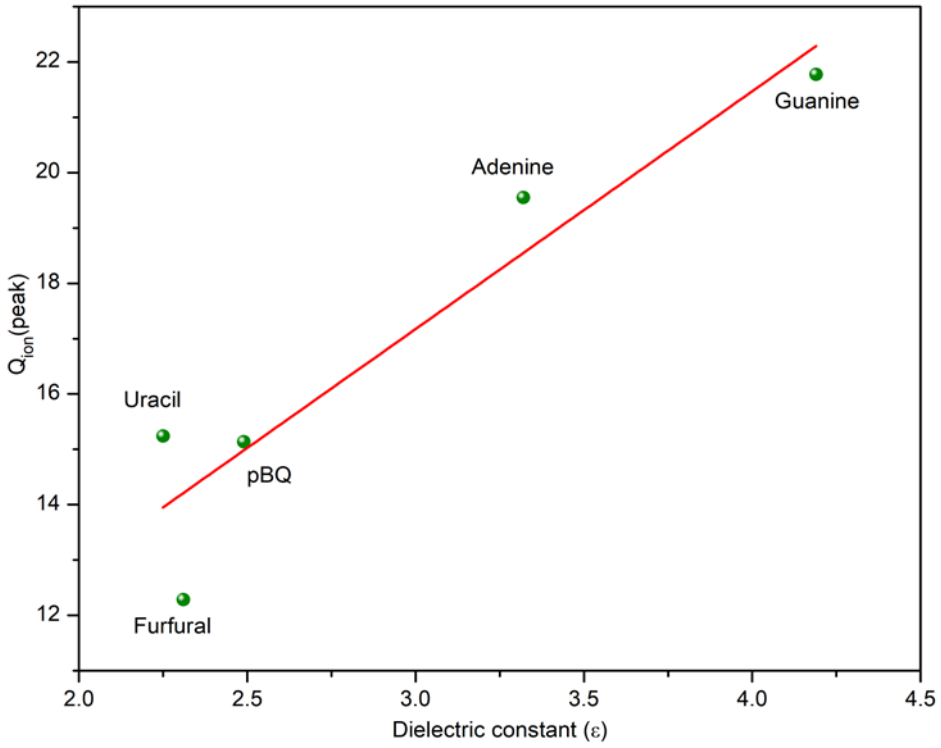

Figure 4.18 Correlation between Q_{ion}^{Max} and ε (through CM eq. 4.1)

Thus, the present investigation of CSs calculation may be helpful to predict dielectric constant for any molecules, as we can see from figure 4.18. It shows a linear correlation exists between the peak ionization cross sections and the dielectric constant as described by the C.M. equation 4.1. For C_3F_5N and C_4F_7N, we use polarizability to compute the N and ε. Also, it's reported in the table 4.10.

Table 4.13 Estimated N and ε

Molecules	**α** **($10^{-24}cm^{-3}$)**	**ρ** g/cm^3	**M** g/mol	**N** $molecules/cm^3$	**ε**
C_3F_5N	5.72 [45]	1.5 [55]	145.03 [55]	$6.2*10^{21}$	1.48
C_4F_7N	6.82 [45]	1.5±0.1 [55]	195.03 [55]	$4.6*10^{21}$	1.31
$C_5F_{10}O$	8.83 [47]	1.53 [55]	266.04 [55]	$3.46*10^{21}$	1.28
$C_6F_{12}O$	11.44 [49]	1.61 [55]	316.04 [55]	$3.06*10^{21}$	1.46

Given the established linear correlation between Q_{ion} (peak) and polarizability [44], as illustrated in figure 4.18, a linear relation of Q_{ion} (peak) with the dielectric constant can be anticipated. Consequently, the present study focused on cross-section computations under electron incident may help in estimating the dielectric constant for diverse materials employed in electronic devices.

J.C. Devins' experiments show that fluoronitriles have double the dielectric strength of SF_6 [56]. C_3F_5N, dielectric constant is used in optimizing composite materials [57]. C_4F_7N, with its superior dielectric properties, also emerges as a promising high-performance insulating gas for electronics equipment, offering a strong alternative to SF_6 [58,59,60].

4.8 Chapter summary

In this chapter we have computed and provides the comprehensive data of elastic, inelastic (including excitation and ionization) and total CSs for electron driven with furfural, para-benzoquinone and Fluoronitriles. These CSs are calculated utilizing the SCOP framework and have been compared with existing literature for energies exceeding the threshold. $C_5H_4O_2$ possesses numerous potential applications within agrochemical sectors, pharmaceuticals, biofuels, and so forth, whereas $C_6H_4O_2$ represents a significant compound in pseudo batteries, artificial photosynthesis, energy storage systems, and the development of novel electronic devices, among others. Due to their high dielectric strength and significantly lower global warming potential (GWP), C_3F_5N and C_4F_7N are promising alternatives to SF_6 for commercial applications, addressing its substantial environmental impact. We also calculated the "dielectric constant (ε)" for all these applied compounds.

Additionally, we have tested the consistency of the method for larger and more complex targets with atomic numbers ranging from 55 to 95. By analyzing existing Q_T for various targets, including DNA constituents, we have observed a strong correlation between the Q_T and ground state target dipole polarizability at intermediate to high energies. Furthermore, we used molecular ionization cross sections and C.M. Onsager to estimate the dielectric constant. Also, we found a number of correlations that could be useful in estimating the dielectric constant and dipole polarizability.

4.9 Bibliography

[1] J. W. Tester, E. M. Drake, M. J. Driscoll, M. W. Golay and W. A. Peters, *Sustainable Energy: Choosing Among Options*, 2nd edition,The MIT Press, Cambridge (2012).

[2] J. Amorim, C. Oliveira, J. A. Souza-Corrêa, and M. A. Ridenti, *Treatment of Sugarcane Bagasse Lignin Employing Atmospheric Pressure Microplasma Jet in Argon*, Plasma Processes and Polymers **10**, 670 (2013).

[3] N. Schultz-Jensen, F. Leipold, H. Bindslev, and A. B. Thomsen, *Plasma-Assisted Pretreatment of Wheat Straw*, Appl Biochem Biotechnol **163**, 558 (2011).

[4] M. A. R. Jayr Amorim, Carlos Oliveira, Jorge A. Souza-Corrêa, *Treatment of Sugarcane Bagasse Lignin Employing Atmospheric Pressure Microplasma Jet in Argon*, Plasma Processes and Polymers **10**, (2013).

[5] M. A. P. L. and M. T. do N. V. Eliane M. de Oliveira, Romarly F. da Costa, Sergio d'A. Sanchez, Alexandra P. P. Natalense, Márcio H. F. Bettega, *Low-Energy Electron Scattering by Cellulose and Hemicellulose Components*, Physical Chemistry Chemical Physics **15**, (2013).

[6] A.S. Mamman, J.-M. Lee, Y.-C. Kim, I.T. Hwang, N.-J. Park, Y.K. Hwang, J.-S. Chang and J.-S. Hwang, *Furfural: Hemicellulose/Xylosederived Biochemical*, Biofuels, Bioprod. Biorefin. **2**, 438–454 (2008).

[7] K. J. Zeitsch, *The Chemistry and Technology of Furfural and Its ManyBy-Products*, 1st edition, Elsevier science (2000).

[8] H. Kobayashi and A. Fukuoka, *Synthesis and Utilisation of Sugar Compounds Derived from Lignocellulosic Biomass*, Green Chemistry **15**, 1740 (2013).

[9] M. A. Ridenti, J. A. Filho, M. J. Brunger, R. F. da Costa, M. T. do N. Varella, M. H. F. Bettega and M. A. P. Lima, *Electron Scattering by Biomass Molecular Fragments: Useful Data for Plasma Applications*, The European Physical Journal D **70**, (2016).

[10] D. B. Jones, R. F. da Costa, M. T. D. N. Varella, M. H. F. Bettega, M. A. P. Lima, F. Blanco, G. García, and M. J. Brunger, *Integral Elastic, Electronic-State, Ionization, and Total Cross Sections for Electron Scattering with Furfural*, Journal of Chemical Physics **144**, (2016).

[11] A. Zouni, H.-T. Witt, J. Kern, P. Fromme and N. Krauss, *Crystal Structure of Photosystem II from Synechococcus Elongatus at 3.8 Å Resolution*, Nature **409**, 739 (2001).

[12] M. Hambourger, G. F. Moore, D.M. Kramer, D. Gust, A.L. Moore and T.A.Moore, *Biology and Technology for Photochemical Fuel Production*, Chemical Society Review **38**, 25 (2009).

[13] O. Yehezkeli, R. Tel-Vered, J. Wasserman, A. Trifonov, D. Michaeli, R. Nechushtai, and I. Willner *Integrated Photosystem II-Based Photo-Bioelectrochemical Cells*, Nat Commun **3**, 742 (2012).

[14] D. B. Jones, F. Blanco, G. García, R. F. Da Costa, F. Kossoski, M. T. D. N. Varella, M. H. F. Bettega, M. A. P. Lima, R. D. White, and M. J. Brunger, *Elastic Scattering and Vibrational Excitation for Electron Impact on Para -Benzoquinone*, Journal of Chemical Physics **147**, (2017).

[15] A. Traoré Dubuis, A. Verkhovtsev, L. Ellis-Gibbings, K. Krupa, F. Blanco, D. B. Jones, M. J. Brunger, and G. García, *Total Cross Section of Furfural by Electron Impact: Experiment and Theory*, Journal of Chemical Physics **147**, (2017).

[16] A. I. Lozano, K. Krupa, F. Ferreira da Silva, P. Limão-Vieira, F. Blanco, A. Muñoz, D. B. Jones, M. J. Brunger, and G. García, *Low Energy Electron Transport in Furfural*, European Physical Journal D **71**, (2017).

[17] A. I. Lozano et al., *Total Electron Scattering Cross Sections from Para -Benzoquinone in the Energy Range 1-200 EV*, Physical Chemistry Chemical Physics **20**, 22368 (2018).

[18] D. B. Jones, R. F. Da Costa, F. Kossoski, M. T. D. N. Varella, M. H. F. Bettega, G. García, F. Blanco, R. D. White, M. A. P. Lima, and M. J. Brunger, *Integral Elastic, Vibrational-Excitation, Electronic-State Excitation, Ionization, and Total Cross Sections for Electron Scattering from Para -Benzoquinone*, Journal of Chemical Physics **148**, (2018).

[19] D. B. Jones, E. Ali, C. G. Ning, J. Colgan, O. Ingólfsson, D. H. Madison, and M. J. Brunger, *Electron Impact Ionization Dynamics of Para -Benzoquinone*, Journal of Chemical Physics **145**, 164306 (2016).

[20] Y. K. Kim and M. E. Rudd, *Binary-Encounter-Dipole Model for Electron-Impact Ionization*, Phys Rev A **50**, 3954 (1994).

[21] G. Garcıa and F. Maneró, *Correlation of the Total Cross Section for Electron Scattering by Molecules with 10-22 Electrons, and Some Molecular Parameters at Intermediate Energies*, Chem Phys Lett **280**, 419 (1997).

[22] X. Li, H. Zhao, and A. B. Murphy, *SF6-Alternative Gases for Application in Gas-Insulated Switchgear*, J Phys D Appl Phys **51**, (2018).

[23] J. D. Mantilla, N. Gariboldi, S. Grob, and M. Claessens, *Investigation of the Insulation Performance of a New Gas Mixture with Extremely Low GWP*, EIC 2014 - Proceedings of the 32nd Electrical Insulation Conference 469 (2014).

[24] X. Zhang, Y. Li, S. Xiao, J. Tang, S. Tian, and Z. Deng, *Decomposition Mechanism of C5F10O: An Environmentally Friendly Insulation Medium*, Environ Sci Technol **51**, 10127 (2017).

[25] J. C. Devins, *Replacement Gases for Sf6*, IEEE Transactions on Electrical Insulation **15**, 81 (1980).

[26] F. Wang, Q. Dun, S. Chen, L. Zhong, X. Fan, and L. L. Li, *Calculations of Total Electron Impact Ionization Cross Sections for Fluoroketone and Fluoronitrile*, IEEE Transactions on Dielectrics and Electrical Insulation **26**, 1693 (2019).

[27] J. Xiong, X. Li, J. Wu, X. Guo, and H. Zhao, *Calculations of Total Electron-Impact Ionization Cross Sections for Fluoroketone C5F10O and Fluoronitrile C4F7N Using Modified Deutsch–Märk Formula*, J Phys D Appl Phys **50**, 445206 (2017).

[28] S. Tian, X. Zhang, S. Xiao, J. Zhang, Q. Chen, and Y. Li, *Application of C6F12O/CO2 Mixture in 10 KV Medium-voltage Switchgear*, Wiley Online Library **13**, 1225 (2019).

[29] M. Vinodkumar, C. Limbachiya, A. Barot, and N. Mason, *Computation of Electron-Impact Rotationally Elastic Total Cross Sections for Methanol over an Extensive Range of Impact Energy (0.1 - 2000 EV)*, Phys Rev A **87**, 012702 (2013).

[30] C. Limbachiya, M. Vinodkumar, and N. Mason, *Calculation of Electron-Impact Rotationally Elastic Total Cross Sections for NH3, H2S, and PH3 over the Energy Range from 0.01 EV to 2 KeV*, Phys Rev A **83**, 042708 (2011).

[31] J. Xiong, X. Li, J. Wu, X. Guo, and H. Zhao, *Calculations of Total Electron-Impact Ionization Cross Sections for Fluoroketone C5F10O and Fluoronitrile C4F7N Using Modified Deutsch-Märk Formula*, J Phys D Appl Phys **50**, 2 (2017).

[32] M. Ranković, J. Chalabala, M. Zawadzki, J. Kočišek, P. Slavíček, and J. Fedor, *Dissociative Ionization Dynamics of Dielectric Gas C3F7CN*, Physical Chemistry Chemical Physics **21**, 16451 (2019).

[33] N. Sinha, V. M. Patel, and B. Antony, *Ionization Cross Sections for Plasma Relevant Molecules*, Journal of Physics B: Atomic, Molecular and Optical Physics **53**, (2020).

[34] F. Wang, Q. Dun, S. Chen, L. Zhong, X. Fan, and L. L. Li, *Calculations of Total Electron Impact Ionization Cross Sections for Fluoroketone and Fluoronitrile*, IEEE Transactions on Dielectrics and Electrical Insulation **26**, 1693 (2019).

[35] Y. K. Kim and P. M. Stone, *Ionization of Boron, Aluminum, Gallium, and Indium by Electron Impact*, Phys Rev A **64**, 11 (2001).

[36] Y. K. Kim and J. P. Desclaux, *Ionization of Carbon, Nitrogen, and Oxygen by Electron Impact*, Phys Rev A **66**, 127081 (2002).

[37] F. Blanco, L. Ellis-Gibbings, and G. García, *Screening Corrections for the Interference Contributions to the Electron and Positron Scattering Cross Sections from Polyatomic Molecules*, Chem Phys Lett **645**, 71 (2016).

[38] D. Chauhan and C. Limbachiya, *Electron Interactions with Analogous of DNA/RNA Nucleobases: 3-HydroxytetrahydroFuran and α-Tetrahydrofurfuryl Alcohol*, Radiation Physics and Chemistry **207**, (2023).

[39] A. Jain, *Spherical-complex-optical-potential (SCOP) Model for Electron–Monosilane (SiH4) Collisions at 30–400 EV: Total (Elastic+absorption), Momentum Transfer, and Differential Cross Sections*, J Chem Phys **86**, 1289 (1987).

[40] L. A. Morgan, J. Tennyson, and C. J. Gillan, *The UK Molecular R-Matrix Codes*, Comput Phys Commun **114**, 120 (1998).

[41] B. I. Schneider and T. N. Rescigno, *Complex Kohn Variational Method: Application to Low-Energy Electron-Molecule Collisions*, Phys Rev A **37**, 3749 (1988).

[42] M. A. P. Lima, L. M. Brescansin, A. J. R. Da Silva, C. Winstead, and V. McKoy, *Applications of the Schwinger Multichannel Method to Electron-Molecule Collisions*, Phys Rev A, **41**, 327 (1990).

[43] M. Vinodkumar, C. Limbachiya, M. Barot, A. Barot, and M. Swadia, *Electron Impact Total Cross Sections for Components of DNA and RNA Molecules*, Int J Mass Spectrom **360**, 1 (2014).

[44] N. Thakkar, M. Swadia, M. Vinodkumar, N. Mason, and C. Limbachiya, *Electron Induced Elastic and Inelastic Processes for Perfluoroketone (PFK) Molecules*, Plasma Sources Sci Technol **30**, (2021).

[45] Y. Wu, C. Wang, H. Sun, A. B. Murphy, M. Rong, F. Yang, Z. Chen, C. Niu, and X. Wang, *Properties of C4F7N-CO2 Thermal Plasmas: Thermodynamic Properties, Transport Coefficients and Emission Coefficients*, J Phys D Appl Phys **51**, (2018).

[46] L. Zhong, J. Wang, X. Wang, and M. Rong, *Calculation of Electron-Impact Ionization Cross Sections of Perfluoroketone (PFK) Molecules CxF2xO (x = 1-5) Based on Binary-Encounter-Bethe (BEB) and Deutsch-Märk (DM) Methods*, Plasma Sources Sci Technol **27**, (2018).

[47] Y. Wu, C. Wang, H. Sun, M. Rong, A. B. Murphy, T. Li, J. Zhong, Z. Chen, F. Yang, and C. Niu, *Evaluation of SF6-Alternative Gas C5-PFK Based on Arc Extinguishing Performance and Electric Strength*, J. Phys. D Appl. Phys. **50**, (2017).

[48] X. Zhang, S. Tian, S. Xiao, Z. Deng, Y. Li, and J. Tang, *Insulation Strength and Decomposition Characteristics of a C6F12O and N2 Gas Mixture*, Energies (Basel) **10**, (2017).

[49] X. Yu, H. Hou, and B. Wang, *Prediction on Dielectric Strength and Boiling Point of Gaseous Molecules for Replacement of SF6*, J Comput Chem **38**, 721 (2017).

[50] M. Bart, P. W. Harland, J. E. Hudson, and C. Vallance, *Absolute Total Electron Impact Ionization Cross-Sections for Perfluorinated Hydrocarbons and Small Halocarbons*, Physical Chemistry Chemical Physics **3**, 800 (2001).

[51] C. Kittel and D. F. Holcomb, *Introduction to Solid State Physics*, 8th ed., **35** (1967).

[52] P. Atkins and J. de Paula, *Physical Chemistry*, Oxford university press (2014).

[53] L. Onsager, *Electric Moments of Molecules in Liquids*, J Am Chem Soc **58**, 1486 (1936).

[54] P. W. Harland and C. Vallance, *Ionization Cross-Sections and Ionization Efficiency Curves from Polarizability Volumes and Ionization Potentials*, Int J Mass Spectrom Ion Process **171**, 173 (1997).

[55] D. P, *CRC Handbook of Chemistry and Physics*, Vol. 268 (CRC Press, 1992).

[56] J. Jiao, D. Xiao, X. Zhao, and Y. Deng, *Analysis of the Molecules Structure and Vertical Electron Affinity of Organic Gas Impact on Electric Strength*, Plasma Science and Technology **18**, 554 (2016).

[57] R. E. Wootton et al., Gases Superior to SF6 for Insulation and Interruption., 1982.

[58] R. Qiu, W. Zhou, Y. Zheng, S. Hu, H. Li, and J. Yu, *A Simulation Research on Diffusion Processes of Discharging Decomposition Products of C4F7N/CO2 in Gas Insulated Transmission Lines*, 7th IEEE International Conference on High Voltage Engineering and Application, ICHVE 2020 - Proceedings 20 (2020).

[59] N. Tang, L. Chen, B. Zhang, and X. Li, *Experimental and Theoretical Exploration of C4F7N Gas Decomposition under Partial Discharge*, 7th IEEE International Conference on High Voltage Engineering and Application, ICHVE 2020 - Proceedings 4 (2020).

[60] J. N. Bull, P. W. Harland, and C. Vallance, *Absolute Total Electron Impact Ionization Cross-Sections for Many-Atom Organic and Halocarbon Species*, Journal of Physical Chemistry A **116**, 767 (2012).